

Probing the predictions of an orbifold theory of flavor

Francisco J. de Anda,^{1,*} Newton Nath,^{2,†} José W. F. Valle,^{3,‡} and Carlos A. Vaquera-Araujo^{4,5,§}

¹*Tepatitlán's Institute for Theoretical Studies, C.P. 47600, Jalisco, México*

²*Instituto de Física, Universidad Nacional Autónoma de México, A.P. 20-364, Ciudad de México 01000, México.*

³*AHEP Group, Institut de Física Corpuscular – C.S.I.C./Universitat de València, Parc Científic de Paterna. C/ Catedrático José Beltrán, 2 E-46980 Paterna (Valencia) - SPAIN*

⁴*Consejo Nacional de Ciencia y Tecnología, Av. Insurgentes Sur 1582. Colonia Crédito Constructor, Del. Benito Juárez, C.P. 03940, Ciudad de México, México*

⁵*Departamento de Física, DCI, Campus León, Universidad de Guanajuato, Loma del Bosque 103, Lomas del Campestre C.P. 37150, León, Guanajuato, México*

We examine the implications of a recently proposed theory of fermion masses and mixings in which an A_4 family symmetry emerges from orbifold compactification. We analyse two variant schemes concerning their predictions for neutrino oscillations, neutrinoless double-beta decay and the golden quark-lepton unification mass relation. We find that upcoming experiments DUNE as well as LEGEND and nEXO offer good chances of exploring a substantial region of neutrino parameters.

I. INTRODUCTION

The discovery of neutrino oscillations [1, 2] has prompted a great experimental effort towards precision measurements [3]. Indeed, the pattern of neutrino mass and mixing parameters is strikingly at odds with the one that characterizes the quark sector, suggesting that it can hardly be expected to happen just by chance. The most popular approach to bring a *rationale* to the pattern of neutrino mixing involves the idea that there is some non-Abelian family symmetry in nature. In a model-independent way one may assume the existence of some residual CP symmetry characterizing the neutrino mass matrix, irrespective of the details of the underlying theory [4–6]. A more ambitious approach is, of course, to guess what the family symmetry actually is, and to build explicit flavor models on a case-by-case basis [7–11]. However, pinning down the nature of such symmetry amongst the plethora of possibilities is a formidable task.

An interesting theoretical idea has been to imagine the existence of new dimensions in space-time, as a way to shed light on the possible nature of the family symmetry in four dimensions. In this context, six-dimensional theories compactified on a torus have been suggested [12, 13] and a realistic standard model extension has recently been proposed [14] in which fermions are nicely arranged within the framework of an A_4 family symmetry. The theory yields very good predictions for fermion masses and mixings, including the “golden” quark-lepton unification formula [15–19].

In this letter we focus on the possibility of probing the implications of this theory within the next generation of neutrino experiments. This includes long-baseline oscillation experiment DUNE [20, 21] as well as neutrinoless double-beta decay ($0\nu\beta\beta$ for short) searches. In Sec. II we describe the theory framework, identifying two model setups, while in Sec. III we determine the potential of upcoming neutrino experiments, such as DUNE and $0\nu\beta\beta$ experiments to probe our orbifold compactification predictions.

* fran@tepaits.mx

† newton@fisica.unam.mx

‡ valle@ific.uv.es

§ vaquera@fisica.ugto.mx

II. THEORY FRAMEWORK

Our model features a 6-dimensional version of the Standard Model $SU(3) \otimes SU(2) \otimes U(1)$ gauge symmetry, together with 3 right handed neutrinos and supplemented with the orbifold compactification described in our previous paper [14]. The transformation properties of the fields under the gauge and A_4 family symmetry and their localization on the orbifold are shown in table I.

Field	$SU(3)$	$SU(2)$	$U(1)$	A_4	Localization
L	1	2	$-1/2$	3	Brane
d^c	$\bar{\mathbf{3}}$	1	$1/3$	3	Brane
e^c	1	1	1	3	Brane
Q	3	2	$1/6$	3	Brane
$u_{1,2,3}^c$	$\bar{\mathbf{3}}$	1	$-2/3$	$\mathbf{1}'', \mathbf{1}', \mathbf{1}$	Bulk
ν^c	1	1	0	3	Brane
H_u	1	2	$1/2$	3	Brane
H_ν	1	2	$1/2$	3	Brane
H_d	1	2	$-1/2$	3	Brane
σ	1	1	0	3	Bulk

TABLE I. Field content of the model.

The scalar sector consists of 3 Higgs doublets and an extra singlet scalar σ , all transforming as flavor triplets. Without loss of generality, we assume that H_d only couples to down type fermions (charged leptons and down quarks), H_u couples only to up quarks and H_ν only couples to neutrinos. The effective Yukawa terms are given by

$$\begin{aligned}
\mathcal{L}_Y = & y^N \nu^c \nu^c \sigma + y_1' (LH_\nu \nu^c)_1 + y_2' (LH_\nu \nu^c)_2 \\
& + y_1^d (Qd^c H_d)_1 + y_2^d (Qd^c H_d)_2 + y_1^e (Le^c H_d)_1 + y_2^e (Le^c H_d)_2 \\
& + y_1^u (QH_u)_{1'} u_1^c + y_2^u (QH_u)_{1''} u_2^c + y_3^u (QH_u)_1 u_3^c,
\end{aligned} \tag{1}$$

where the symbol $(\)_{1,2}$ indicates the possible singlet contractions $\mathbf{3} \times \mathbf{3} \times \mathbf{3} \rightarrow \mathbf{1}_{1,2}$ and $\mathbf{3} \times \mathbf{3} \rightarrow \mathbf{1}_{1,1',1''}$ in A_4 . All dimensionless Yukawa couplings are assumed to be real due to a CP symmetry.

The scalar field σ gets a vacuum expected value (VEV) that breaks spontaneously lepton number and the A_4 family symmetry, giving large Majorana masses to the right handed neutrinos. The corresponding VEV is aligned as

$$\langle \sigma \rangle = v_\sigma \begin{pmatrix} 1 \\ \omega \\ \omega^2 \end{pmatrix}, \tag{2}$$

with $\omega = e^{2\pi i/3}$, the cube root of unity.

As A_4 is broken at a high mass scale, the Higgs doublets can obtain the most general spontaneous CP violating alignment, which we parametrize as

$$\langle H_u \rangle = v_u \begin{pmatrix} \epsilon_1^u e^{i\phi_1^u} \\ \epsilon_2^u e^{i\phi_2^u} \\ 1 \end{pmatrix}, \quad \langle H_\nu \rangle = v_\nu e^{i\phi^\nu} \begin{pmatrix} \epsilon_1^\nu e^{i\phi_1^\nu} \\ \epsilon_2^\nu e^{i\phi_2^\nu} \\ 1 \end{pmatrix}, \quad \langle H_d \rangle = v_d e^{i\phi^d} \begin{pmatrix} \epsilon_1^d e^{i\phi_1^d} \\ \epsilon_2^d e^{i\phi_2^d} \\ 1 \end{pmatrix}. \tag{3}$$

An important prediction of the model comes from the fact that the charged leptons and down-quarks obtain their masses from the same H_d , so that the A_4 structure implies the golden relation between their masses [15]

$$\frac{m_\tau}{\sqrt{m_\mu m_e}} = \frac{m_b}{\sqrt{m_s m_d}}, \tag{4}$$

This relation is in good agreement with experiments [22] and is rather robust against renormalization group running.

The explicit form of the mass matrices for the matter fields (up to unphysical rephasings) is given as

$$\begin{aligned}
M_u &= v_u \begin{pmatrix} y_1^u \epsilon_1^u & y_2^u \epsilon_1^u & y_3^u \epsilon_1^u \\ y_1^u \epsilon_2^u \omega^2 & y_2^u \epsilon_2^u \omega & y_3^u \epsilon_2^u \\ y_1^u \omega & y_2^u \omega^2 & y_3^u \end{pmatrix}, \\
M_d &= v_d \begin{pmatrix} 0 & y_1^d \epsilon_1^d e^{i(\phi_1^d - \phi_2^d)} & y_2^d \epsilon_2^d \\ y_2^d \epsilon_1^d e^{i(\phi_1^d - \phi_2^d)} & 0 & y_1^d \\ y_1^d \epsilon_2^d & y_2^d & 0 \end{pmatrix}, \\
M_e &= v_d \begin{pmatrix} 0 & y_1^e \epsilon_1^d e^{-i(\phi_1^d - \phi_2^d)} & y_2^e \epsilon_2^d \\ y_2^e \epsilon_1^d e^{-i(\phi_1^d - \phi_2^d)} & 0 & y_1^e \\ y_1^e \epsilon_2^d & y_2^e & 0 \end{pmatrix}, \\
M_N^R &= y^N v_\sigma \begin{pmatrix} 0 & \omega^2 & \omega \\ \omega^2 & 0 & 1 \\ \omega & 1 & 0 \end{pmatrix}, \\
M_\nu^D &= v_\nu \begin{pmatrix} 0 & y_1^\nu \epsilon_1^\nu e^{i(\phi_1^\nu - \phi_2^\nu)} & y_2^\nu \epsilon_2^\nu \\ y_2^\nu \epsilon_1^\nu e^{i(\phi_1^\nu - \phi_2^\nu)} & 0 & y_1^\nu \\ y_1^\nu \epsilon_2^\nu & y_2^\nu & 0 \end{pmatrix}, \\
M_\nu^L &= M_\nu^D (M_N^R)^{-1} (M_\nu^D)^T.
\end{aligned} \tag{5}$$

In what follows we adopt the standard parameterization for the Cabibbo-Kobayashi-Maskawa (CKM) matrix

$$V_{CKM} = \begin{pmatrix} c_{12}^q c_{13}^q & s_{12}^q c_{13}^q & s_{13}^q e^{-i\delta^q} \\ -s_{12}^q c_{23}^q - c_{12}^q s_{13}^q s_{23}^q e^{i\delta^q} & c_{12}^q c_{23}^q - s_{12}^q s_{13}^q s_{23}^q e^{i\delta^q} & c_{13}^q s_{23}^q \\ s_{12}^q s_{23}^q - c_{12}^q s_{13}^q c_{23}^q e^{i\delta^q} & -c_{12}^q s_{23}^q - s_{12}^q s_{13}^q c_{23}^q e^{i\delta^q} & c_{13}^q c_{23}^q \end{pmatrix}, \tag{6}$$

and the symmetrical presentation of the lepton mixing matrix [23, 24],

$$K = \begin{pmatrix} c_{12}^\ell c_{13}^\ell & s_{12}^\ell c_{13}^\ell e^{-i\phi_{12}} & s_{13}^\ell e^{-i\phi_{13}} \\ -s_{12}^\ell c_{23}^\ell e^{i\phi_{12}} - c_{12}^\ell s_{13}^\ell s_{23}^\ell e^{-i(\phi_{23} - \phi_{13})} & c_{12}^\ell c_{23}^\ell - s_{12}^\ell s_{13}^\ell s_{23}^\ell e^{-i(\phi_{23} + \phi_{12} - \phi_{13})} & c_{13}^\ell s_{23}^\ell e^{-i\phi_{23}} \\ s_{12}^\ell s_{23}^\ell e^{i(\phi_{23} + \phi_{12})} - c_{12}^\ell s_{13}^\ell c_{23}^\ell e^{i\phi_{13}} & -c_{12}^\ell s_{23}^\ell e^{i\phi_{23}} - s_{12}^\ell s_{13}^\ell c_{23}^\ell e^{-i(\phi_{12} - \phi_{13})} & c_{13}^\ell c_{23}^\ell \end{pmatrix}, \tag{7}$$

with $c_{ij}^f \equiv \cos \theta_{ij}^f$ and $s_{ij}^f \equiv \sin \theta_{ij}^f$ where $f = q, \ell$. The advantage of using the symmetrical parameterization for the lepton mixing matrix resides in the transparent role of the Majorana phases in the effective mass parameter characterizing the amplitude for neutrinoless double beta decay

$$\langle m_{\beta\beta} \rangle = \left| \sum_{j=1}^3 K_{ej}^2 m_j \right| = \left| c_{12}^{\ell 2} c_{13}^{\ell 2} m_1 + s_{12}^{\ell 2} c_{13}^{\ell 2} m_2 e^{2i\phi_{12}} + s_{13}^{\ell 2} m_3 e^{2i\phi_{13}} \right|, \tag{8}$$

while keeping a rephasing-invariant expression for the Dirac phase

$$\delta^\ell = \phi_{13} - \phi_{12} - \phi_{23} \tag{9}$$

which affects neutrino oscillation probabilities.

A. Model Set-up I (MI)

Following [14], we may further assume that the Higgs's VEVs preserve conventional (trivial) CP symmetry, and therefore they are real. Together with the reality of the Yukawa couplings, this implies that the only source of CP violation is the phase ω . This leads to a very strong predictivity.

The model is specified by 15 parameters ($y_{1,2}^\nu v_\nu, y_{1,2}^{e,d} v_d, y_{1,2,3}^u v_u, \epsilon_{1,2}^{u,\nu,d}$) that describe 22 low-energy flavor observables: ($m_{u,c,t,d,s,b,e,\mu,\tau}, m_{1,2,3}^\nu, \theta_{12,13,23}^q, \delta^q, \theta_{12,13,23}^l, \phi_{12,13,23}$) including the neutrino Majorana phases. One extra parameter ($y^N v_\sigma$) defines the masses of the 3 right handed neutrinos.

Parameter	Value	Observable	Data		Model best fit
			Central value	1 σ range	
$y_1^e v_d/\text{GeV}$	1.745	$\theta_{12}^l / ^\circ$	34.44	33.46 \rightarrow 35.67	34.36
$y_2^e v_d/(10^{-1}\text{GeV})$	-1.019	$\theta_{13}^l / ^\circ$	8.45	8.31 \rightarrow 8.61	8.31
$y_1^d v_d/(10^{-2}\text{GeV})$	-4.690	$\theta_{23}^l / ^\circ$	47.69	45.97 \rightarrow 48.85	48.47
$y_2^d v_d/\text{GeV}$	2.88	$\delta^l / ^\circ$	237	210 \rightarrow 275	268
$y_1^\nu v_\nu/\sqrt{Y^N v_\sigma \text{meV}} \times 10^{-1}$	7.54	m_e / MeV	0.489	0.489 \rightarrow 0.489	0.489
$y_2^\nu v_\nu/(\sqrt{Y^N v_\sigma \text{meV}} \times 10^{-3})$	1.89	m_μ / GeV	0.102	0.102 \rightarrow 0.102	0.102
$y_1^u v_u/(10^{-1}\text{GeV})$	6.24	m_τ / GeV	1.745	1.743 \rightarrow 1.747	1.745
$y_2^u v_u/(10^2\text{GeV})$	1.71	$\Delta m_{21}^2/(10^{-5} \text{eV}^2)$	7.55	7.39 \rightarrow 7.75	7.63
$y_3^u v_u/\text{GeV}$	-7.13	$\Delta m_{31}^2/(10^{-3} \text{eV}^2)$	2.50	2.47 \rightarrow 2.53	2.42
$\epsilon_1^u/10^{-4}$	-6.90	m_1 / meV			4.12
$\epsilon_2^u/10^{-2}$	6.24	m_2 / meV			9.66
$\epsilon_1^d/10^{-3}$	-2.74	m_3 / meV			50.11
$\epsilon_2^d/10^{-3}$	6.00	$\phi_{12} / ^\circ$			250
ϵ_1^ν	1.16	$\phi_{13} / ^\circ$			187
$\epsilon_2^\nu/10^{-1}$	-3.23	$\phi_{23} / ^\circ$			29
		$\theta_{12}^q / ^\circ$	13.04	12.99 \rightarrow 13.09	13.04
		$\theta_{13}^q / ^\circ$	0.20	0.19 \rightarrow 0.22	0.20
		$\theta_{23}^q / ^\circ$	2.38	2.32 \rightarrow 2.44	2.37
		$\delta^q / ^\circ$	68.75	64.25 \rightarrow 73.25	60.25
		m_u / MeV	1.28	0.76 \rightarrow 1.55	1.29
		m_c / GeV	0.626	0.607 \rightarrow 0.645	0.626
		m_t / GeV	171.6	170 \rightarrow 173	171.6
		m_d / MeV	2.74	2.57 \rightarrow 3.15	2.75
		m_s / MeV	54	51 \rightarrow 57	51
		m_b / GeV	2.85	2.83 \rightarrow 2.88	2.91
		χ^2			12.4

TABLE II. Global best-fit of flavor observables within **MI**. Here CP violation is generated by a fixed phase ω .

One can perform a global fit to the flavor observables by defining the chi-square function

$$\chi^2 = \sum (\mu_{exp} - \mu_{model})^2 / \sigma_{exp}^2, \quad (10)$$

where the sum runs through the 19 measured physical parameters (note that the overall neutrino mass scale and the two Majorana phases are currently undetermined). We make use of the MPT package [25] to obtain the flavor observables from the mass matrices in Eq. (5). Then we scan the 15 free parameters and find the values that minimize the χ^2 function. Neutrino oscillation parameters are taken from the global fit in Ref. [3], while the rest of the observables are taken from the PDG [22]. For consistency of the fit, all quark and charged lepton masses are evolved to the same common scale, which we choose to be M_Z . The running of CKM and neutrino mixing parameters is negligible [26, 27]. The results are shown in table II. One sees from the fit that $\chi^2 = 12.4$. This indicates a relatively good global fit, with some tension in the description of quark CP violation, as seen from the table. The origin for this is traced to the absence of a free parameter describing CP violation, as discussed above.

B. Model Set-up II (MII)

We can now relax the assumption that all the Higgs VEVs are real, allowing them to be general complex numbers. However, we keep the assumption that the Yukawa couplings are real. This reinstates 2 physical phases $\phi_1^{\nu,d} - \phi_2^{\nu,d}$, now increasing to the number of free parameters to 17, for a total of 22 flavor observables.

Parameter	Value	Data		Model best fit
		Central value	1σ range	
$y_1^e v_d / (10^{-1} \text{ GeV})$	-1.020			
$y_2^e v_d / \text{ GeV}$	1.745			
$y_1^d v_d / (10^{-2} \text{ GeV})$	-5.069			
$y_2^d v_d / \text{ GeV}$	2.869			
$y_1^\nu v_\nu / \sqrt{Y^N v_\sigma} \text{ meV}$	-1.461			
$y_2^\nu v_\nu / \sqrt{Y^N v_\sigma} \text{ meV}$	7.647			
$y_1^u v_u / (10^{-1} \text{ GeV})$	6.198			
$y_2^u v_u / (10^2 \text{ GeV})$	1.712			
$y_3^u v_u / \text{ GeV}$	7.143			
$\epsilon_1^u / 10^{-4}$	-6.926			
$\epsilon_2^u / 10^{-2}$	-5.058			
$\epsilon_1^d / 10^{-3}$	2.812			
$\epsilon_2^d / 10^{-3}$	5.863			
$\epsilon_1^\nu / 10^{-1}$	-9.950			
$\epsilon_2^\nu / 10^{-1}$	5.979			
$(\phi_1^d - \phi_2^d) / \pi$	-1.078			
$(\phi_1^\nu - \phi_2^\nu) / \pi$	1.093			
Observable		Central value	1σ range	Model best fit
$\theta_{12}^\ell / ^\circ$		34.44	33.46 \rightarrow 35.67	34.65
$\theta_{13}^\ell / ^\circ$		8.45	8.31 \rightarrow 8.61	8.44
$\theta_{23}^\ell / ^\circ$		47.69	45.97 \rightarrow 48.85	47.56
$\delta^\ell / ^\circ$		237	210 \rightarrow 275	198.3
$m_e / \text{ MeV}$		0.489	0.489 \rightarrow 0.489	0.489
$m_\mu / \text{ GeV}$		0.102	0.102 \rightarrow 0.102	0.102
$m_\tau / \text{ GeV}$		1.745	1.743 \rightarrow 1.747	1.745
$\Delta m_{21}^2 / (10^{-5} \text{ eV}^2)$		7.55	7.39 \rightarrow 7.75	7.55
$\Delta m_{31}^2 / (10^{-3} \text{ eV}^2)$		2.50	2.47 \rightarrow 2.53	2.42
$m_1 / \text{ meV}$				24.31
$m_2 / \text{ meV}$				25.81
$m_3 / \text{ meV}$				55.60
$\phi_{12} / ^\circ$				252.5
$\phi_{13} / ^\circ$				142.3
$\phi_{23} / ^\circ$				51.5
$\theta_{12}^q / ^\circ$		13.04	12.99 \rightarrow 13.09	13.04
$\theta_{13}^q / ^\circ$		0.20	0.19 \rightarrow 0.22	0.20
$\theta_{23}^q / ^\circ$		2.38	2.32 \rightarrow 2.44	2.38
$\delta^q / ^\circ$		68.75	64.25 \rightarrow 73.25	69.25
$m_u / \text{ MeV}$		1.28	0.76 \rightarrow 1.81	1.29
$m_c / \text{ GeV}$		0.626	0.607 \rightarrow 0.645	0.626
$m_t / \text{ GeV}$		171.6	170 \rightarrow 173	171.6
$m_d / \text{ MeV}$		2.74	2.35 \rightarrow 3.15	2.51
$m_s / \text{ MeV}$		54	51 \rightarrow 57	54
$m_b / \text{ GeV}$		2.85	2.76 \rightarrow 2.94	2.87
χ^2				1.6

TABLE III. Global best-fit of flavor observables within **MI**. Here there are two free CP violation phases.

In this general setup, we loose predictivity for the physical CP violating phases $\delta^{l,q}$, leading to a drastic improvement of the global fit, achieving a minimum $\chi^2 = 1.6$ as seen in the table **III**. Notice now the very good agreement of all of the observables, including the value of the CKM CP violation phase δ^q .

As mentioned above, a characteristic feature of our schemes is the golden quark-lepton mass relation given in Eq. 4. We now turn to study this prediction as obtained from our global fits of flavor observables within Models I and II. In Fig. 1 we use the golden quark-lepton mass relation in **MI** and **MII** to make predictions for the down and strange quark masses. Here the cyan bands stand for the 1, 2 and 3σ regions compatible with the exact golden relation $m_\tau / \sqrt{m_\mu m_e} = m_b / \sqrt{m_s m_d}$ at the M_Z scale, and the yellow contours are the 1, 2 and 3σ regions for the quark mass parameters measured at the same scale. To better appreciate the predictive power of our framework, we have varied randomly the parameters of **MII** around the best fit point in Table III and we have determined the shape of the parameter region consistent at 3σ with all the 19 measured parameters of the model. This region is shown in purple in Fig. 1. The corresponding contour for **MI** is not shown as it is very similar, given the fact that the golden relation is not very sensitive to the improvement of the CP violating phases in **MII**, compared to **MI**. However, one can see

that the best fit point for scheme **MII**, indicated by the black cross, is now compatible at 1σ with the exact golden formula.

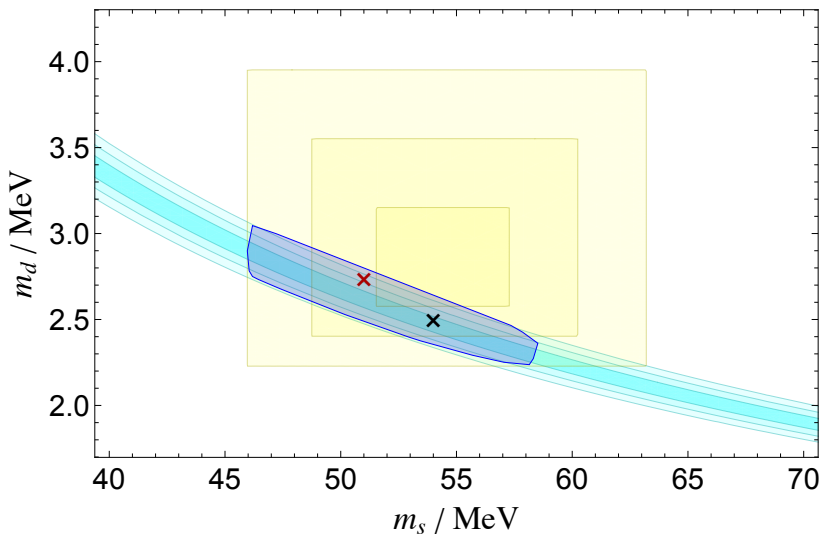


FIG. 1. Prediction for the down-quark and strange-quark masses at the M_Z scale. The cyan contours represent the 1, 2 and 3σ allowed regions from the golden relation $m_\tau/\sqrt{m_\mu m_e} = m_b/\sqrt{m_s m_d}$. The yellow contours show the 1, 2 and 3σ ranges of the measured quark masses at the M_Z scale [27]. The blue region is the allowed parameter space consistent at 3σ with the global flavour fit in Table III. The red (black) cross indicates the location of the best fit point for **MI** (**MII**).

III. PROBING NEUTRINO PREDICTIONS

In this section we present a close-up of the neutrino predictions of our orbifold compactification schemes, examining also the capability of future experiments to test them.

A. Neutrino oscillations at DUNE

We start by quantifying the capability of the DUNE experiment to test the oscillation predictions resulting from the A_4 family symmetry, as realized from a six-dimensional spacetime after orbifold compactification. Before presenting details about the simulated results, we first give a brief technical overview of the simulation details of DUNE, the proposed next generation superbeam neutrino oscillation experiment at Fermilab, USA [20, 21]. The collaboration plans to use neutrinos from the Main Injector (NuMI) at Fermilab as a neutrino source. In this experiment, the first detector will record particle interactions near the beam source, at Fermilab. On the other hand, the neutrinos from Fermilab will travel a distance of 1300 km before reaching the far detector situated at the underground laboratory of “Sanford Underground Research Facility (SURF)” in Lead, South Dakota. The proposed far detector will use four 10 kton volume of liquid argon time-projection chambers (LArTPC). The expected neutrino flux corresponding to 1.07 MW beam power gives 1.47×10^{21} protons on target (POT) per year for an 80 GeV proton beam energy. We follow the same procedure as given in [28] for performing our numerical analysis of DUNE. The GLOBES package [29, 30] along with the auxiliary files as mentioned in [21] has been utilized for the simulation. We adopt 3.5 years running time in both neutrino and antineutrino modes, with a 40 kton total detector volume. In the numerical analysis, we also take into account both the appearance and disappearance channels of neutrinos and antineutrinos. In addition, both the signal and background normalization uncertainties for the appearance as well as disappearance channels have been taken into account in our analysis, as mentioned in the DUNE CDR [21].

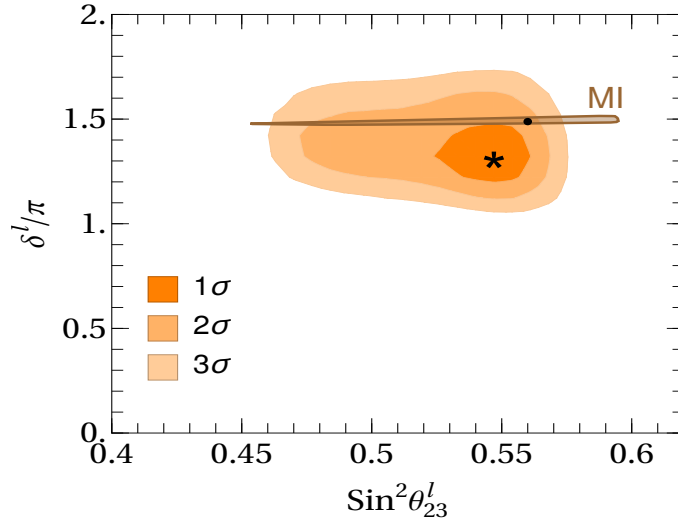


FIG. 2. DUNE sensitivity region in the $(\sin^2 \theta_{23}^l, \delta^l)$ plane. The ‘star-mark’ represents the latest neutrino oscillation best-fit [3], while the ‘black-dot’ is the predicted best-fit, as given in Table II.

Given that normal mass ordering (i.e., $m_1 < m_2 < m_3$) of neutrinos is currently preferred over the inverted one (i.e., $m_3 < m_1 < m_2$) at more than 3σ [3], we focus on the first scenario throughout this work.

In what follows, we examine the sensitivity regions of DUNE in the $(\sin^2 \theta_{23}^l, \delta^l)$ for different seed points. These are shown at 1σ (dark-orange), 2σ (orange), and 3σ (lighter-orange) confidence level, respectively.

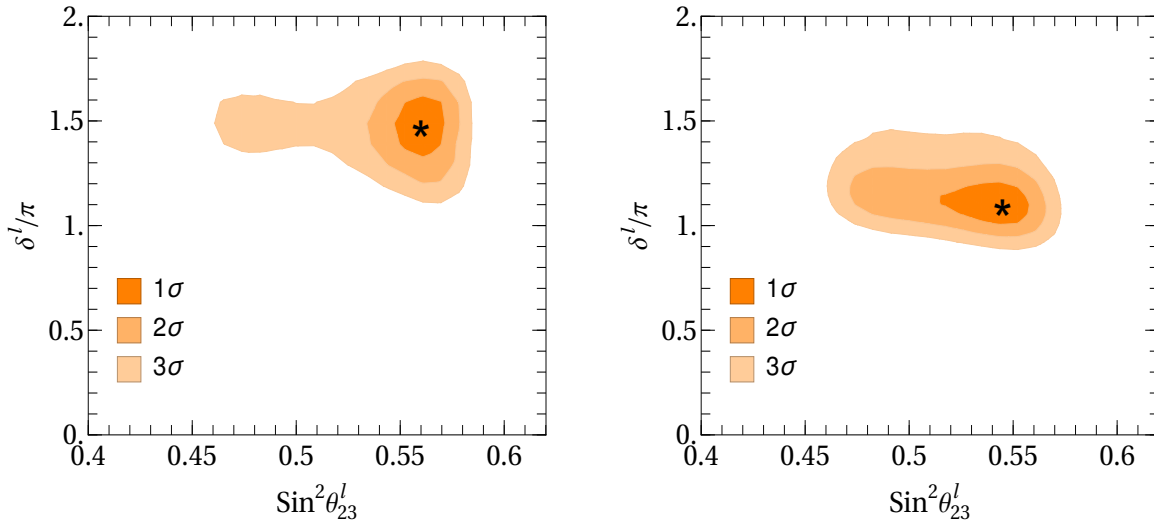


FIG. 3. DUNE $(\sin^2 \theta_{23}, \delta)$ sensitivity regions in models **MI** (left) and **MI** (right), assuming the corresponding best-fit points obtained in setup **MI** (left-panel) and **MI** (right-panel), respectively, as indicated by the ‘star-marks’.

In Fig. 2, we show the expected $1, 2$ and 3σ DUNE sensitivity regions in the $(\sin^2 \theta_{23}^l, \delta^l)$ plane. Here we assume model setup **MI** and take the latest neutrino oscillation best-fit point from [3] as benchmark, as indicated by the black ‘star-mark’. The corresponding **MI** theory predictions are indicated by the brown 3σ confidence level region, and its best-fit point, as given in Table II, is shown by the black ‘dot’. One sees that DUNE will be able to rule out predicted correlation between $\sin^2 \theta_{23}^l$, and δ^l for **MI** at 1σ C. L. In contrast, we note that the predicted region in model **MI** covers the full DUNE sensitivity contours, so we do not show this plot in Fig. 2. In other words, if the

current best fit value of the oscillation parameters remains, DUNE will not be able to rule out the predictions for **MII** even at 1σ C. L.

We now change our seed points, adopting as benchmarks the $(\sin^2 \theta'_{23}, \delta^l)$ best-fit points predicted in each of the models described above. The resulting DUNE sensitivity regions are given in Fig. 3.

One sees from the left-panel that, if the **MI** predicted value of $(\sin^2 \theta'_{23}, \delta^l)$ is the true benchmark value, then DUNE (after 3.5 running time in both neutrino and antineutrino modes) can rule out maximal value of θ'_{23} i.e., $\sin^2 \theta'_{23} = \pi/2$ at 2σ confidence level. On the other hand, by adopting the **MII** predicted best-fit as the true seed value, we notice from the right-panel that DUNE can rule out maximal value of $\sin^2 \theta'_{23}$ at 1σ , whereas it can rule out $\delta^l = 3\pi/2$ at 3σ confidence level.

B. Neutrinoless double-beta decay

We now turn to the predictions for neutrinoless double beta decay in Models **MI** and **MII** and confront them with experimental sensitivities [31–38]. This is shown in Fig. 4. The values for the effective mass $\langle m_{\beta\beta} \rangle$ consistent at 3σ with the measured flavor observables (mainly neutrino oscillation parameters) obtained from the global fit are represented by the green contour for the case of the “constrained” model **MI**, and by the blue one for **MII**. The theory-predicted regions are obtained by allowing the free parameters to vary randomly from the best fit point while simultaneously complying at 3σ with all the measured observables of the global fit. One sees that the predicted region for **MII** becomes wider, while the region for **MI** remains quite small. This is due to the effect of the variation of the available free phases in **MII** $\phi_1^{\nu,d} - \phi_2^{\nu,d}$, which are directly related to the Majorana phases. In contrast, in **MI** the

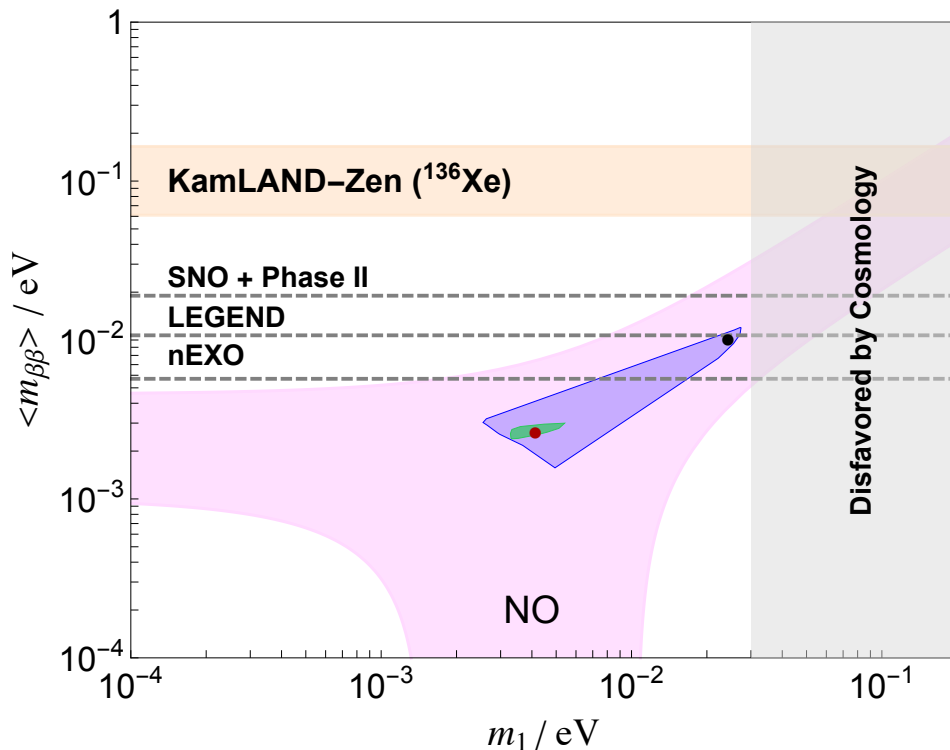


FIG. 4. Effective Majorana neutrino mass parameter $\langle m_{\beta\beta} \rangle$ as a function of the lightest active neutrino mass m_1 . Here green (blue) contour represents the predicted $\langle m_{\beta\beta} \rangle$ parameter space consistent at 3σ with the global flavor fit for model setup **MI** (**MII**), and the best-fit value is shown by the red (black) dot. The current KamLAND-Zen limit is shown by the light-yellow band, and the projected sensitivities for future experiments are indicated in dashed horizontal lines, see text for details.

only available CP violating phase is fixed, leading to sharply predicted $0\nu\beta\beta$ decay amplitude which can not deviate much from its best fit value.

Interestingly enough, predictivity is not destroyed by the inclusion of those extra phases, and **MII** still has upper and lower bounds for both the effective mass $\langle m_{\beta\beta} \rangle$ and the lightest neutrino mass parameter. As a visual guide for the experimental searches of $0\nu\beta\beta$, in Fig. 4 the horizontal yellow band indicates the current experimental limits from Kamland-Zen (61 – 165 meV) [31], while the dashed lines correspond to the most optimistic sensitivities projected for SNO + Phase II (19 – 46 meV) [35], LEGEND (10.7 – 22.8 meV) [36], and nEXO (5.7 – 17.7 meV) [37]. One sees that the best fit point for MII, marked with a black point, becomes testable by the next generation of $0\nu\beta\beta$ experiments LEGEND and nEXO. Finally, the vertical gray band represents the current sensitivity of cosmological data from the Planck collaboration [39].

IV. CONCLUSION

We have investigated the implications of a recently proposed theory of fermion masses and mixings based on an A_4 family symmetry that arises from the compactification of a 6-dimensional orbifold. We have analysed two variants of the idea, a “constrained” one in which CP violation is strictly predicted, and another where CP phases are free to vary. We have quantified the predictions of these schemes for neutrino oscillations, neutrinoless double-beta decay and the golden quark-lepton mass formula. We have found that the projected long baseline experiment DUNE can probe the model predictions concerning the maximality of the atmospheric mixing or the value of the CP phase in a meaningful way. Likewise, the next generation of neutrinoless double-beta decay experiments, especially LEGEND and nEXO, could probe our model **MII** in a substantial region of parameters.

ACKNOWLEDGMENTS

Work supported by the Spanish grants SEV-2014-0398 and FPA2017-85216-P (AEI/FEDER, UE), PROMETEO/2018/165 (Generalitat Valenciana) and the Spanish Red Consolider MultiDark FPA2017-90566-REDC. CAV-A is supported by the Mexican Cátedras CONACYT project 749 and SNI 58928. NN is supported by the postdoctoral fellowship program DGAPA-UNAM, CONACYT CB-2017-2018/A1-S-13051 (México) and DGAPA-PAPIIT IN107118.

-
- [1] T. Kajita, “Nobel Lecture: Discovery of atmospheric neutrino oscillations,” *Rev.Mod.Phys.* **88** (2016) 030501.
 - [2] A. B. McDonald, “Nobel Lecture: The Sudbury Neutrino Observatory: Observation of flavor change for solar neutrinos,” *Rev.Mod.Phys.* **88** (2016) 030502.
 - [3] P. de Salas *et al.*, “Status of neutrino oscillations 2018: 3σ hint for normal mass ordering and improved CP sensitivity,” *Phys.Lett.* **B782** (2018) 633–640, [arXiv:1708.01186 \[hep-ph\]](#).
 - [4] P. Chen *et al.*, “Generalized $\mu - \tau$ reflection symmetry and leptonic CP violation,” *Phys.Lett.* **B753** (2016) 644–652, [arXiv:1512.01551 \[hep-ph\]](#).
 - [5] P. Chen *et al.*, “Classifying CP transformations according to their texture zeros: theory and implications,” *Phys.Rev.* **D94** (2016) 033002, [arXiv:1604.03510 \[hep-ph\]](#).
 - [6] P. Chen *et al.*, “CP symmetries as guiding posts: Revamping tribimaximal mixing. II.,” *Phys. Rev.* **D100** no. 5, (2019) 053001, [arXiv:1905.11997 \[hep-ph\]](#).
 - [7] K. Babu, E. Ma, and J. W. F. Valle, “Underlying $A(4)$ symmetry for the neutrino mass matrix and the quark mixing matrix,” *Phys.Lett.* **B552** (2003) 207–213.
 - [8] G. Altarelli and F. Feruglio, “Discrete Flavor Symmetries and Models of Neutrino Mixing,” *Rev.Mod.Phys.* **82** (2010) 2701–2729, [arXiv:1002.0211 \[hep-ph\]](#).

- [9] S. Morisi and J. W. F. Valle, “Neutrino masses and mixing: a flavour symmetry roadmap,” *Fortsch.Phys.* **61** (2013) 466–492, [arXiv:1206.6678 \[hep-ph\]](#).
- [10] S. F. King, A. Merle, S. Morisi, Y. Shimizu, and M. Tanimoto, “Neutrino Mass and Mixing: from Theory to Experiment,” *New J.Phys.* **16** (2014) 045018, [arXiv:1402.4271 \[hep-ph\]](#).
- [11] P. Chen *et al.*, “Warped flavor symmetry predictions for neutrino physics,” *JHEP* **1601** (2016) 007, [arXiv:1509.06683 \[hep-ph\]](#).
- [12] F. J. de Anda and S. F. King, “An $S_4 \times SU(5)$ SUSY GUT of flavour in 6d,” *JHEP* **1807** (2018) 057, [arXiv:1803.04978 \[hep-ph\]](#).
- [13] F. J. de Anda and S. F. King, “ $SU(3) \times SO(10)$ in 6d,” *JHEP* **1810** (2018) 128, [arXiv:1807.07078 \[hep-ph\]](#).
- [14] F. J. de Anda, J. W. F. Valle, and C. A. Vaquera-Araujo, “Flavour and CP predictions from orbifold compactification,” *Phys.Lett.* **B801** (2020) 135195, [arXiv:1910.05605 \[hep-ph\]](#).
- [15] S. Morisi *et al.*, “Relating quarks and leptons without grand-unification,” *Phys.Rev.* **D84** (2011) 036003, [arXiv:1104.1633 \[hep-ph\]](#).
- [16] S. King *et al.*, “Quark-Lepton Mass Relation in a Realistic A_4 Extension of the Standard Model,” *Phys.Lett.* **B724** (2013) 68–72, [arXiv:1301.7065 \[hep-ph\]](#).
- [17] S. Morisi *et al.*, “Quark-Lepton Mass Relation and CKM mixing in an A_4 Extension of the Minimal Supersymmetric Standard Model,” *Phys.Rev.* **D88** (2013) 036001, [arXiv:1303.4394 \[hep-ph\]](#).
- [18] C. Bonilla *et al.*, “Relating quarks and leptons with the T_7 flavour group,” *Phys.Lett.* **B742** (2015) 99–106, [arXiv:1411.4883 \[hep-ph\]](#).
- [19] M. Reig, J. W. Valle, and F. Wilczek, “ $SO(3)$ family symmetry and axions,” *Phys.Rev.* **D98** (2018) 095008, [arXiv:1805.08048 \[hep-ph\]](#).
- [20] **DUNE** Collaboration, R. Acciarri *et al.*, “Long-Baseline Neutrino Facility (LBNF) and Deep Underground Neutrino Experiment (DUNE),” [arXiv:1512.06148 \[physics.ins-det\]](#).
- [21] **DUNE** Collaboration, T. Alion *et al.*, “Experiment Simulation Configurations Used in DUNE CDR,” [arXiv:1606.09550 \[physics.ins-det\]](#).
- [22] **Particle Data Group** Collaboration, M. Tanabashi *et al.*, “Review of Particle Physics,” *Phys.Rev.* **D98** (2018) 030001.
- [23] J. Schechter and J. W. F. Valle, “Neutrino Masses in $SU(2) \times U(1)$ Theories,” *Phys.Rev.* **D22** (1980) 2227.
- [24] W. Rodejohann and J. W. F. Valle, “Symmetrical Parametrizations of the Lepton Mixing Matrix,” *Phys.Rev.* **D84** (2011) 073011, [arXiv:1108.3484 \[hep-ph\]](#).
- [25] S. Antusch, J. Kersten, M. Lindner, M. Ratz, and M. A. Schmidt, “Running neutrino mass parameters in see-saw scenarios,” *JHEP* **0503** (2005) 024.
- [26] Z.-z. Xing, H. Zhang, and S. Zhou, “Updated Values of Running Quark and Lepton Masses,” *Phys.Rev.* **D77** (2008) 113016, [arXiv:0712.1419 \[hep-ph\]](#).
- [27] S. Antusch and V. Maurer, “Running quark and lepton parameters at various scales,” *JHEP* **1311** (2013) 115, [arXiv:1306.6879 \[hep-ph\]](#).
- [28] N. Nath, R. Srivastava, and J. W. F. Valle, “Testing generalized CP symmetries with precision studies at DUNE,” *Phys.Rev.* **D99** (2019) 075005, [arXiv:1811.07040 \[hep-ph\]](#).
- [29] P. Huber, M. Lindner, and W. Winter, “Simulation of long-baseline neutrino oscillation experiments with GLOBES (General Long Baseline Experiment Simulator),” *Comput.Phys.Commun.* **167** (2005) 195.
- [30] P. Huber, J. Kopp, M. Lindner, M. Rolinec, and W. Winter, “New features in the simulation of neutrino oscillation experiments with GLOBES 3.0: General Long Baseline Experiment Simulator,” *Comput.Phys.Commun.* **177** (2007) 432–438.
- [31] **KamLAND-Zen** Collaboration, A. Gando *et al.*, “Search for Majorana Neutrinos near the Inverted Mass Hierarchy Region with KamLAND-Zen,” *Phys.Rev.Lett.* **117** (2016) 082503, [arXiv:1605.02889 \[hep-ex\]](#).
- [32] **CUORE** Collaboration, C. Alduino *et al.*, “First Results from CUORE: A Search for Lepton Number Violation via $0\nu\beta\beta$ Decay of ^{130}Te ,” *Phys.Rev.Lett.* **120** (2018) 132501, [arXiv:1710.07988 \[nucl-ex\]](#).
- [33] **EXO** Collaboration, J. Albert *et al.*, “Search for Neutrinoless Double-Beta Decay with the Upgraded EXO-200 Detector,” *Phys.Rev.Lett.* **120** (2018) 072701, [arXiv:1707.08707 \[hep-ex\]](#).
- [34] **GERDA** Collaboration, M. Agostini *et al.*, “Improved Limit on Neutrinoless Double- β Decay of ^{76}Ge from GERDA Phase II,” *Phys.Rev.Lett.* **120** (2018) 132503, [arXiv:1803.11100 \[nucl-ex\]](#).
- [35] **SNO+** Collaboration, S. Andringa *et al.*, “Current Status and Future Prospects of the SNO+ Experiment,” *Adv.High*

- Energy Phys.* **2016** (2016) 6194250, [arXiv:1508.05759](#) [[physics.ins-det](#)].
- [36] **LEGEND** Collaboration, N. Abgrall *et al.*, “The Large Enriched Germanium Experiment for Neutrinoless Double Beta Decay (LEGEND),” vol. 1894, p. 020027. 2017. [arXiv:1709.01980](#) [[physics.ins-det](#)].
- [37] **nEXO** Collaboration, J. Albert *et al.*, “Sensitivity and Discovery Potential of nEXO to Neutrinoless Double Beta Decay,” *Phys.Rev.* **C97** (2018) 065503, [arXiv:1710.05075](#) [[nucl-ex](#)].
- [38] O. Azzolini *et al.*, “Search for Neutrino-less Double Beta Decay of ^{64}Zn and ^{70}Zn with CUPID-0,” [arXiv:2003.10840](#) [[nucl-ex](#)].
- [39] **Planck** Collaboration, N. Aghanim *et al.*, “Planck 2018 results. VI. Cosmological parameters,” [arXiv:1807.06209](#) [[astro-ph.CO](#)].